ACS APPLIED MATERIALS & INTERFACES

www.acsami.org

Research Article

# Biocompatible Nanotransfer Printing Based on Water Bridge Formation in Hyaluronic Acid and Its Application to Smart Contact Lenses

Jiwoo Ko, Hyeok Joong Kang, Junseong Ahn, Zhi-Jun Zhao, Yongrok Jeong, Soon Hyoung Hwang, Moonjeong Bok, Sohee Jeon, Jimin Gu, Ji-Hwan Ha, Junsuk Rho, Jun-Ho Jeong,* and Inkyu Park*

Cite This: *ACS Appl. Mater. Interfaces* 2021, 13, 35069–35078

Read Online

ACCESS | Metrics & More | Article Recommendations | Supporting Information

**ABSTRACT:** Many conventional micropatterning and nanopatterning techniques employ toxic chemicals, rendering them nonbiocompatible and unsuited for biodevice production. Herein the formation of water bridges on the surface of hyaluronic acid (HA) films is exploited to develop a transfer-based nanopatterning method applicable to diverse structures and materials. The HA film surface, made deformable via water bridge generation, is brought into contact with a functional material and subjected to thermal treatment, which results in film shrinkage, allowing a robust pattern transfer. The proposed biocompatible method, which avoids the use of extra chemicals, enables the transfer of nanoscale, microscale, and thin-film structures as well as functional materials such as metals and metal oxides. A nanopatterned HA film is transferred onto a moisture-containing contact lens to fabricate smart contact lenses with unique optical characteristics of rationally designed optical nanopatterns. These lenses demonstrated binocular parallax-induced stereoscopy via nanoline array polarization and acted as cutoff filters, with nanodot arrays, capable of treating Irlen syndrome.

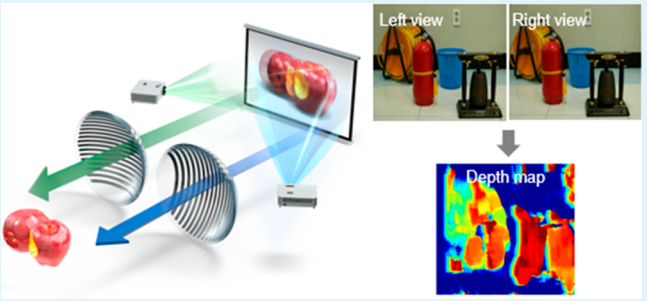


**KEYWORDS:** *hyaluronic acid, nanotransfer printing, smart contact lens, stereoscopy, cutoff filter*

## INTRODUCTION

Biodevices, including wearable, implantable, and minimally invasive types, are used to monitor the vital signs of a human body,[1−3] deliver drugs, and treat diseases.[4−6] They are commonly fabricated using micro- and nanopatterning techniques, which allow improved performance, miniaturization, and mechanical flexibility. For example, micropatterns can be used as serpentine electrodes that can be attached onto curved surfaces, such as those of organs or blood vessels,[7,8] while nanopatterns can be employed as waveguides and diffraction grating reflectors in implantable photonic devices.[9] Further progress in the design of wearable and implantable biodevices requires the development of biocompatible materials and fabrication processes. Widely used micro- and nanopatterning methods include photolithography,[3] nanoimprinting lithography,[10] electron-beam (e-beam) lithography,[11] and nanotransfer printing.[12] Among these, lithographic techniques such as nanoimprinting lithography, e-beam lithography, and extreme ultraviolet lithography are nonbiocompatible, costly, require toxic chemicals, and inflict material damage due to light exposure. In contrast, the nanotransfer printing processes, which utilize the surface energy difference between the donor and receiver substrates, are highly biocompatible, particularly when biofriendly materials are used. Among the various available biomaterials, hyaluronic acid (HA) has excellent biocompatibility and biodegradability, as reflected by its certification by the Food and Drug Administration, and is a promising component of biocompatible wearable and implantable devices. In particular, HA has been widely used in osteoarthritis treatment, cosmetics production, plastic surgery, tissue engineering, and drug delivery,[13−17] and it has potential application in the fabrication of wearable or implantable devices using micro/nanopatterning. However, most of the reported HA patterning techniques rely on molding.[12,18,19] A recently reported nanotransfer patterning method uses an HA nanotemplate, in which the HA nanopatterns are fabricated via HA solution nanomolding, for nanotransfer patterning of functional materials (FMs).[12] However, this method suffers from nonselective deposition of functional films on the HA nanotemplate, making it difficult to

Received: April 5, 2021
Accepted: July 12, 2021
Published: July 20, 2021

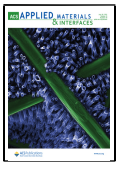

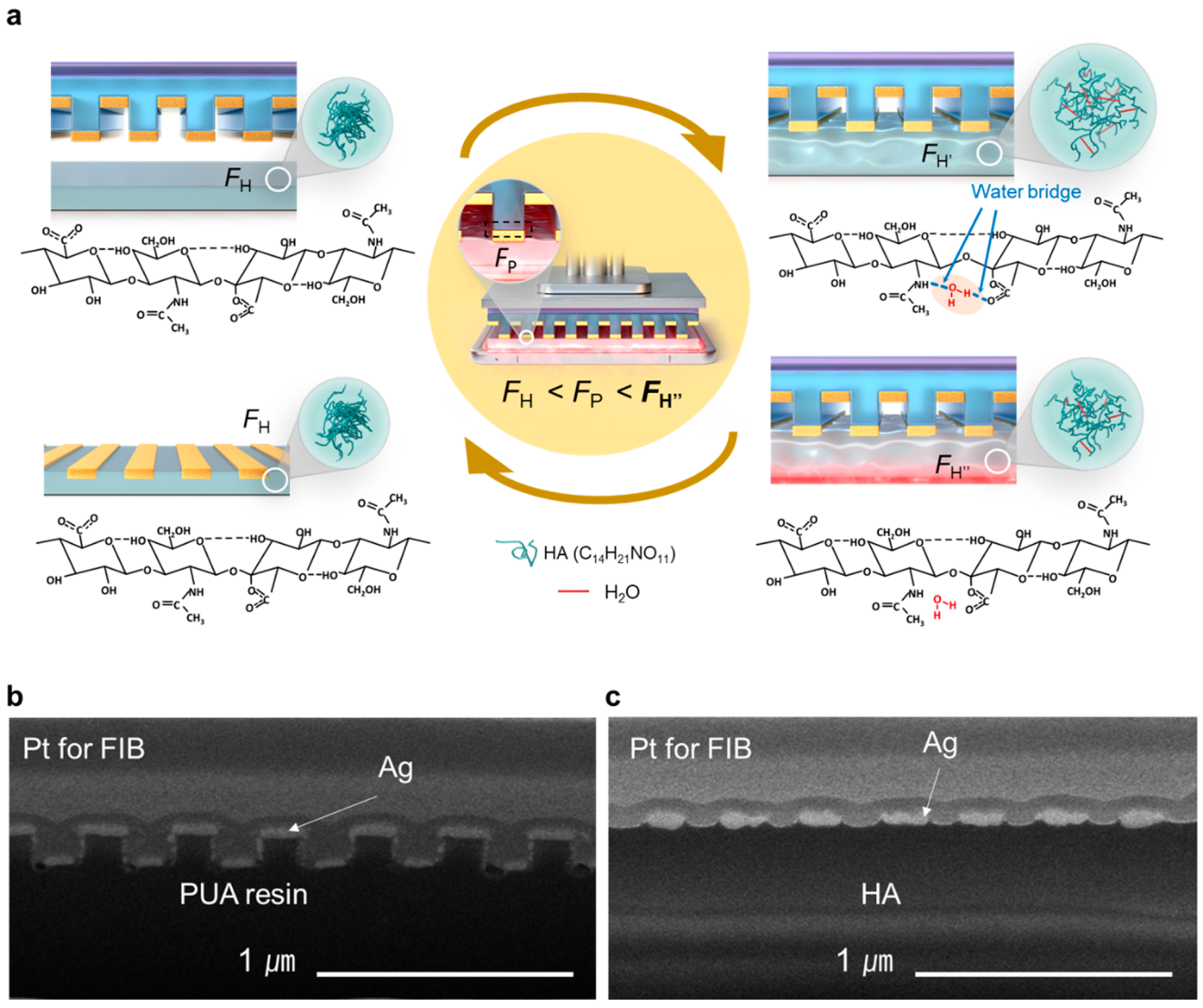


**Figure 1.** Nanotransfer printing on HA film based on water bridge formation. (a) Schematic illustration of the mechanism of the proposed method: (1) Initial state of the HA film; (2) formation of water bridges between polymer chains via attraction of ambient water and the application of pressure to achieve a conformal contact; (3) evaporation of water from the polymer chain upon heating; (4) shrinkage of the HA film and transfer of FM patterns onto the HA film. SEM image of the (b) polymer mold with an Ag thin film (pattern of dots with $D/P$ = 180 nm/340 nm) and (c) result of the transfer of the Ag nanopatterns onto the HA film.

precisely control the optical properties of the transferred nanopatterns.

In this study, the inherent ability of HA to attract water from its environment was exploited to transfer nanopatterns, micropatterns, and thin-film structures of FMs onto a flat HA substrate without using additional chemicals, such as adhesives, thereby fabricating biocompatible devices with precisely controlled optical properties. Specifically, the HA film binds water from ambient air to create water bridges between the polymer chains, thereby enhancing its deformability. The hydrated HA film is brought in contact with the FM and subjected to thermal treatment, which results in water bridge breakage and film shrinkage, inducing mechanical interlocking between the HA and FM and allowing the transfer of the latter with high mechanical robustness. The developed method, which allows the transfer of various nanoscale to mesoscale FM patterns onto HA films, was used for the nanotransfer printing of rationally designed optical nanopatterns onto a moisture-containing contact lens to develop a smart contact lens with unique optical characteristics. The resulting optical lens demonstrated its potential for two optical applications, namely (i) binocular parallax-assisted stereoscopy via nanoline array polarization and (ii) as a cutoff filter with a nanodot array for the treatment of Irlen syndrome.

## RESULTS AND DISCUSSION

**Nanotransfer Printing Based on Water Bridge Formation.** HA is a hydrophilic linear polysaccharide that comprises D-glucuronic acid connected to *N*-acetyl-D-glucosamine as a disaccharide repeating unit and can absorb ambient moisture, allowing each skin cell to retain water more than 1000-fold its weight.[15,16] The proposed method relies on the transfer of variable dimension patterns of diverse materials to a hydrated HA substrate (Figure 1a) and features several stages:[15] HA (Figure 1a-1) attracts ambient water vapor (red rods in Figure 1a-2) to form water bridges between polymer


https://doi.org/10.1021/acsami.1c06225
ACS Appl. Mater. Interfaces 2021, 13, 35069−35078

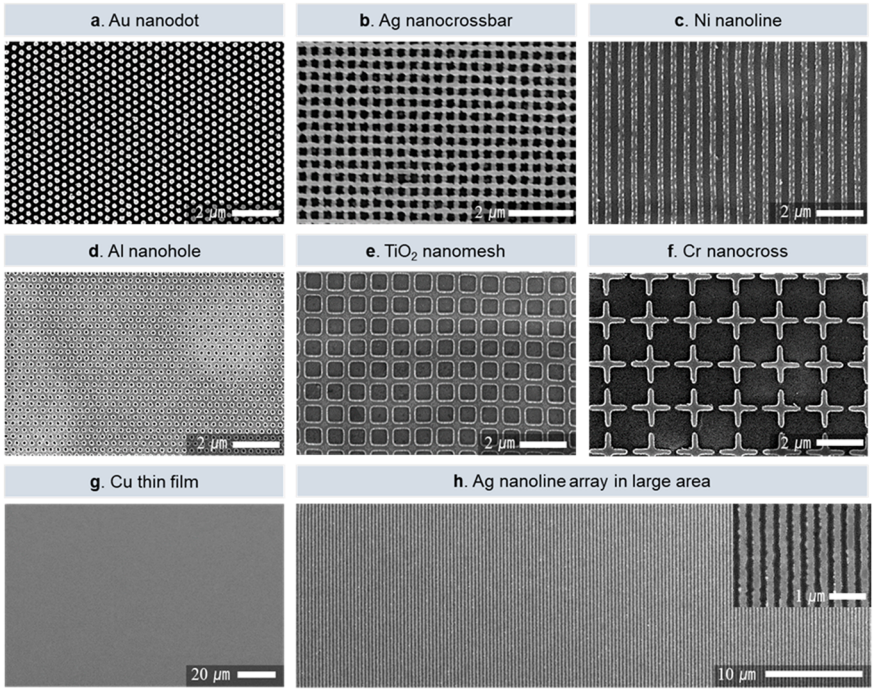


**Figure 2.** SEM images showing the results of transferring nanopatterns of various materials onto HA films. (a) Au nanodot array with $D/P$ = 200 nm/500 nm. (b) Ag nanocrossbar stacked layer with $L/S$ = 200 nm/200 nm. (c) Ni nanoline array with $L/S$ = 200 nm/400 nm. (d) Al nanohole array with $D/P$ = 180 nm/340 nm. (e) $TiO_2$ nanomesh hole array with $L/S$ = 200 nm/800 nm. (f) Cr nanocross array with a line width of 200 nm and length of 1.6 $\mu$m. (g) Cu thin film. (h) Ag nanoline array with $L/S$ = 200 nm/200 nm in a large area.

chains.[15] The hydrated HA film was overlaid with a polyurethane acrylate (PUA) film with FM patterns, subjected to pressure to achieve a conformal contact. It was then heated to evaporate the water (Figure 1a-3) and subsequently induce film shrinkage, which allows the transfer of the FM pattern (Figure 1a-4).

The formation of numerous water bridges between the HA polymer chains results in swelling and increases the content of surface hydroxyl groups,[20−22] making the HA substrate soft, deformable, and sticky, thereby facilitating FM attachment. To facilitate transfer of the FM to the hydrated HA film, the adhesion between the FM and this film ($F_H$) should be stronger than that between the FM and the PUA mold ($F_P$). Materials with low $F_P$, such as Ag nanopatterned materials, can be easily transferred to HA films even at room temperature at a pressure <10 kPa,[23] whereas materials with $F_P > F_H$ (e.g., Au, Al, and Cr) cannot be transferred to HA films using the original difference in adhesion strength only.

To strengthen the adhesion between the HA film and FM, heat can be applied to remove the water from the polymer chains and subsequently induce volumetric shrinkage. This shrinkage leads to mechanical interlocking between the HA film and FM, making $F_H$ exceed $F_P$ and allowing the transfer of most FMs. If the original HA film does not have a sufficient moisture content, then the volumetric shrinkage is small and $F_H$ remains lower than $F_P$. In this case, the FMs cannot be transferred to the HA film, even by applying high temperature and pressure (Figure S1). In addition, most materials either cannot be transferred or can only be partially transferred at room temperature because volumetric shrinkage and mechanical interlocking cannot be induced at room temperature. Therefore, the proposed process utilizes the appropriate moisture content, to initially generate abundant water bridges, and sufficient thermal energy, to break these bridges, to induce mechanical interlocking via volumetric shrinkage.

The transfer process occurred in an aqueous environment with neutral pH conditions. Therefore, it can be expected that the ionic dissolution from the FM film is very small. In addition, the maximum time and temperature of the transfer process were ∼5 min and ∼100 °C, respectively. Consequently, FM mobilization within the HA film is expected to be negligible. To analyze the chemical composition of the transferred interface, high-resolution SEM-EDS was performed (Figure S2). From the results, it can be assumed that the transferred functional material does not further diffuse into the HA film and exists only on the surface.

Figure 1b shows a cross-sectional scanning electron microscopy (SEM) image of the Ag nanodot patterns (diameter/pitch ($D/P$) = 180 nm/340 nm) deposited on a PUA mold, while Figure 1c shows an SEM image of the Ag nanopatterns transferred from the PUA mold to the HA film. The transferred pattern was slightly embedded into the HA film due to the mechanical interlocking taking place during the heat-induced water bridge cleavage and volumetric shrinkage. From the transferred shape, the FM and the HA film were strongly bonded, and a peel test and scratch test were performed to confirm the bonding strength (Figure S3). For the peel test, tapes of various strengths were used; however, none of the used tapes allowed pattern transfer of FM from the HA film. This implies that the HA film and FM were well-bonded with sufficient strength. In the scratch test, pattern damage in a particular trajectory occurred because of using a sharp metallic tool such as a tweezer, which damaged the HA film as well as the nanopattern. In addition to this, there were some areas where the pattern was partially removed when rubbed strongly by hand; however, most patterns remained


https://doi.org/10.1021/acsami.1c06225
ACS Appl. Mater. Interfaces 2021, 13, 35069−35078

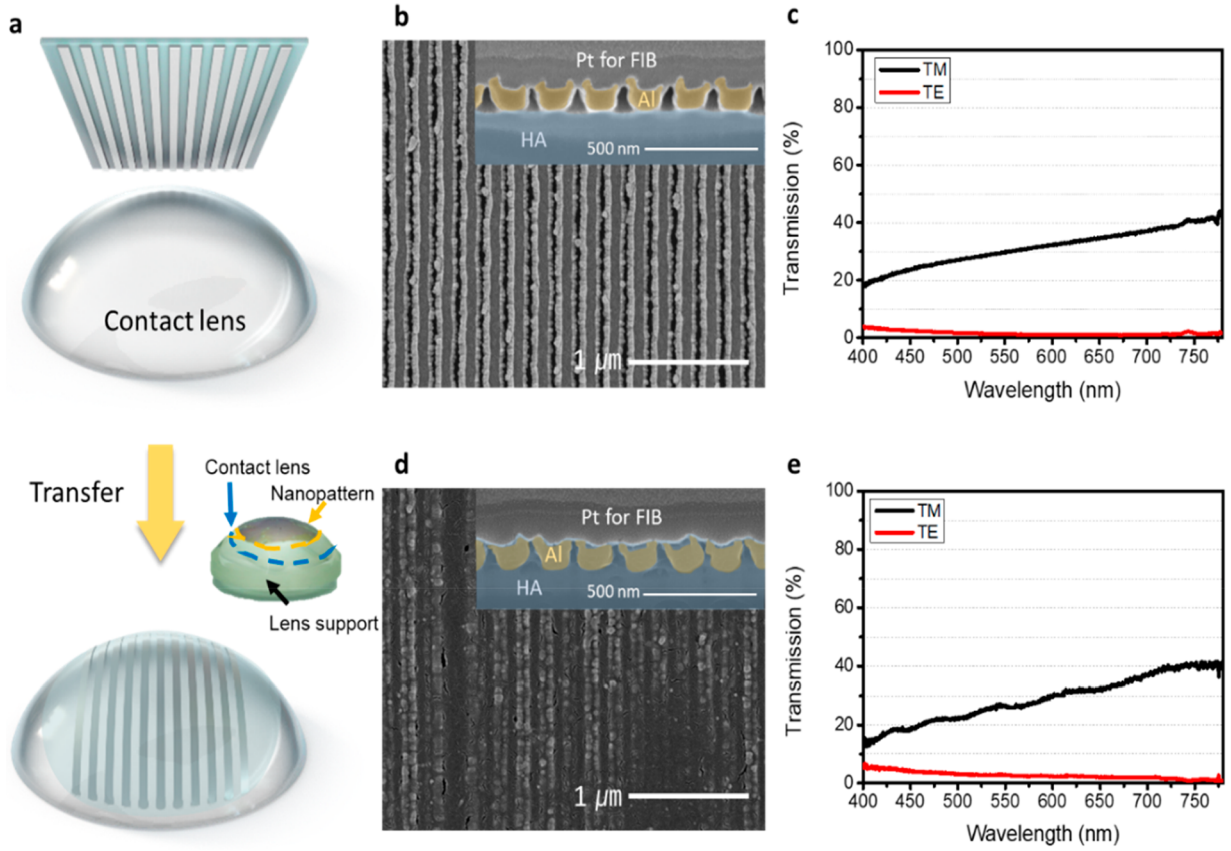


**Figure 3.** Nanopatterned contact lens obtained by HA film transfer. (a) Fabrication using a water-soluble nanotemplate on a contact lens. The inset shows the fabricated lens. (b) SEM image of Al nanopatterned HA film with $L/S$ = 100 nm/100 nm, and (c) the related transmission curves for TM and TE modes. (d) SEM image of the nanopatterned contact lens obtained when the HA film was (b) transferred to the contact lens, and (e) the related transmission curves for TM and TE modes.

unchanged. These results indicate that the HA film and FM were very strongly bonded to each other.

The proposed method was applied to transfer various materials (e.g., Au, Ag, Ni, Al, Cr, Cu, and $TiO_2$), nanoscale patterns with unique optical characteristics (e.g., dots, holes, and meshes), microscale patterns (e.g., crosses), and thin films (Figure 2). The nanoline patterns of various materials with a line width/spacing ($L/S$) of 200 nm/400 nm were successfully transferred, as shown in the related cross-sectional images and transfer results in Figures S4 and S5. Furthermore, several layers could also be stacked by transferring new layers onto a pre-existing layer (e.g., a crossbar structure was obtained by stacking two nanoline patterns perpendicularly, as shown in Figure 2b). Nanowelding, caused by nanoscale melting-point depression, allows stacking at low temperatures in the range of 90−120 °C.[24] Figure 2h shows an SEM image of a sample transferred onto a 2″ diameter HA film. Additional SEM images obtained at five different points on the patterned HA film reveal the uniformity of the entire area (Figure S6).

**Fabrication of Nanopatterned Contact Lens.** The ability of HA to attract ambient water was used to transfer an HA film, with functional nanopatterns, to a contact lens (Figures 3a and S7), thereby obtaining a smart contact lens with unique optical functionality. Previous studies related to smart contact lenses employed various methods, e.g., fabrication of a pattern on a transparent film and its incorporation onto a soft lens,[25−27] pattern transfer after photolithography,[25−31] laser interference patterning,[32,33] and near-field subdiffraction photolithography.[34] The smart lenses resulting from these processes are used for glucose-level measurement,[25,31,34−37] intraocular pressure measurement,[27−29,38−40] dry eye prevention,[41,42] and color blindness correction.[43,44] The process developed in this study was employed to transfer an HA film, nanopatterned with an Al nanoline array, onto a hydrogel-based soft contact lens made of narafilcon A with a water content of 46 wt %.[45,46]

The success of this transfer was confirmed by cross-sectional SEM imaging and transmission spectroscopy analysis of the patterns before and after the film transfer (Figure 3b−e). Figure 3b and 3c shows the SEM images and polarized transmission spectra of the Al nanoline array on the HA film prior to transfer. Polarization refers to the direction in which the electric and magnetic fields oscillate during electromagnetic wave propagation. The polarization direction of an electromagnetic wave is generally defined by the direction of the electric field oscillation and can be categorized as transverse electric (TE) and transverse magnetic (TM). In the TE mode, the electric field oscillates along the direction of the Al nanoline array and the free electrons of the metal can move freely in this direction. This results in the reflection of the polarized light, similar to the reflection of light on a metallic surface. Conversely, in the TM mode, the motion of the free electrons of the metal is confined to a narrow region and light is transmitted through the nanostructure without reflection. In this study, the polarization extinction ratio (TM/TE) of the fabricated film was approximately 38 at ∼670 nm. Figure 3d


https://doi.org/10.1021/acsami.1c06225
ACS Appl. Mater. Interfaces 2021, 13, 35069−35078

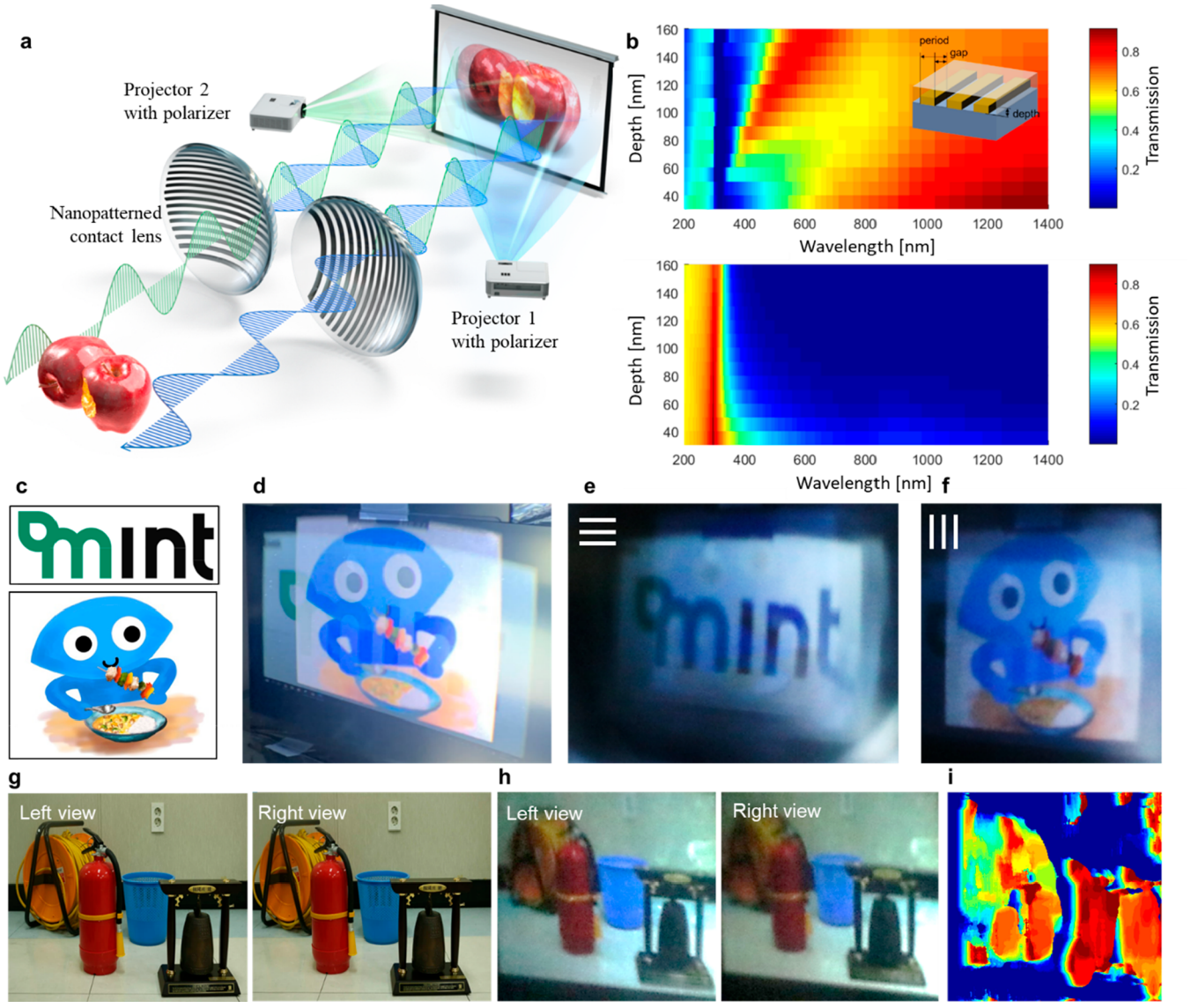


**Figure 4.** Stereoscopic contact lens based on polarization-based binocular parallax: (a) Concept of stereoscopy based on the use of a nanopatterned contact lens. (b) Simulation results obtained in the TM (upper) and TE (lower) modes for an Al nanoline array with $L/S$ = 100 nm/100 nm. (c–f) Experimental results of the polarization-dependent image transmission using two different images: (c) Two images used for demonstration. (d) Overlapped state. Transmitted images obtained when the lens pattern was aligned in the (e) horizontal and (f) vertical directions. Binocular parallax experiment performed according to the polarization mode: (g) input images obtained from the left and right directions of the same object and (h) the result of transmitting them through the polarized lens. (i) Depth map obtained using panel h as the input images. Red color denotes objects that are closer to the lens.

shows an SEM image of the Al nanoline array after it was transferred onto the soft contact lens. As the lens surface was covered with a thick (~20 $\mu$m) HA layer, it was difficult to obtain a clear cross-sectional image of the transferred patterns using a focused ion beam (FIB) (Figure S8). Therefore, for better visualization of the transferred patterns, they were separated from the soft contact lens by quenching in liquid nitrogen. The result shows that the Al nanoline pattern maintained its original spacing after being transferred onto the curved lens surface. The Al nanoline pattern was surrounded by HA, which was partially hydrated by the moisture of the contact lens and could easily penetrate the regions between the patterns to facilitate the lens–pattern bonding. As presented in Figure 3e, the nanoline array pattern on the contact lens exhibited polarization characteristics similar to those of the pattern on the HA film before the transfer (Figure 3c). Notably, there was no additional water supplied during the transfer, i.e., only the inherent moisture of the contact lens was used. After transfer, the lens and pattern were firmly fixed and coated with an HA layer to produce a smart contact lens that is resistant to rubbing and scratching and could maintain its original optical characteristics for more than three months.

**Binocular Parallax-Assisted Stereoscopy via Nanoline Array Polarization.** As mentioned previously, the prepared smart contact lens was used in two practical demonstrations, one of which was to perform binocular parallax-assisted stereoscopy via nanoline array polarization.

Among the different strategies for realizing stereoscopy, using a polarized three-dimensional (3D) system, obtained via binocular parallax, is the most popular method. In this case, a single surface, comprising two overlapped images, is employed to achieve 3D visualization using binocular parallax when


https://doi.org/10.1021/acsami.1c06225
ACS Appl. Mater. Interfaces 2021, 13, 35069–35078

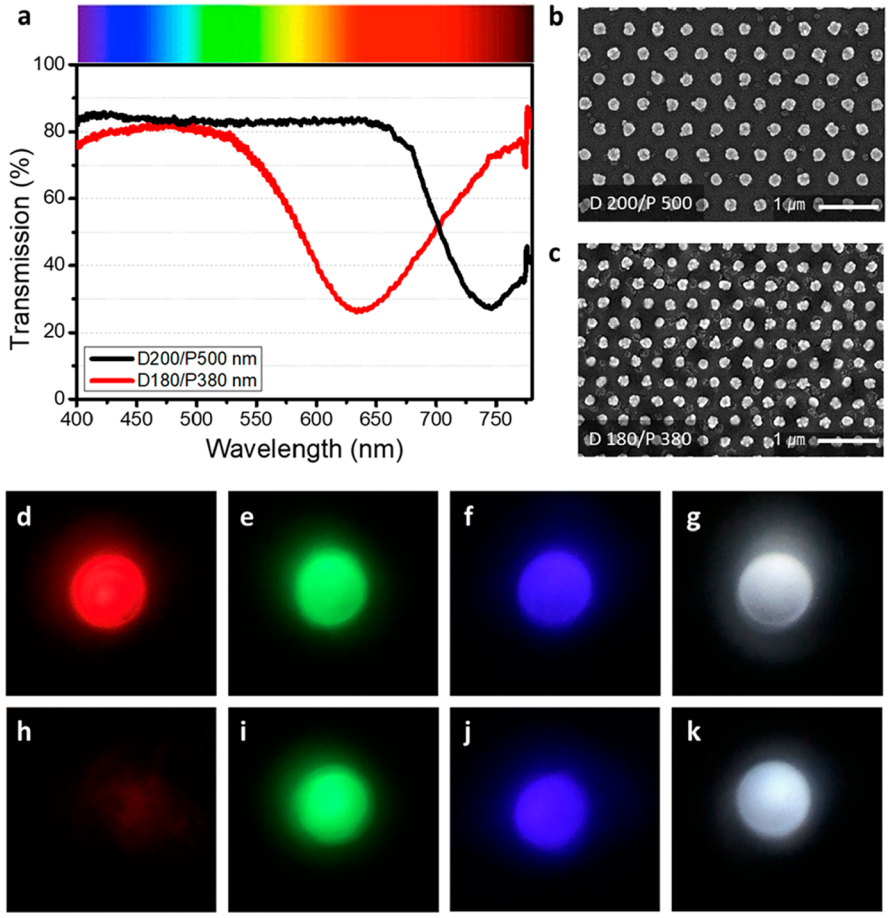


**Figure 5.** Specific wavelength of the cutoff filter formed by a nanodot array-patterned contact lens. (a) Transmission curves of the nanopatterned contact lenses with $D/P$ = 200 nm/500 and 180 nm/380 nm. The black curve corresponds to the transmission of a Ag nanodot array with $D/P$ = 200 nm/500 nm and $t$ = 50 nm. The red curve shows the transmission of a Ag nanodot array with $D/P$ = 180 nm/380 nm and $t$ = 50 nm. SEM image of nanopatterned HA films with (b) $D/P$ = 200 nm/500 nm and (c) 180 nm/380 nm. Red, green, blue, and white light transmitted through (d–g) a conventional contact lens without nanopatterns, respectively, and (h–k) a nanopatterned contact lens with $D/P$ = 180 nm/380 nm, respectively.

different images are seen by the left and right eyes (Figure 4a). To realize binocular parallax via polarization, one image should be transmitted in the entire visible region, while the other image must be blocked so that different images can be seen by each eye.

The pattern size and material were selected through finite-difference time-domain (FDTD) simulations to obtain an effective polarizer structure. Increasing the pattern size resulted in the partial transmission of visible light (Figure S9a,b). Accordingly, the pattern with an $L/S$ of 100 nm/100 nm was selected as the optimal pattern. The properties of Ag and Al, which are common materials for preparing metallic patterns with desirable optical effects, were compared. Ag exhibits a sharper optical peak than Al and allows partial transmission of visible light, whereas Al has a relatively even transmission in this wavelength region (Figure S9c,d). Therefore, Al was chosen as the nanoline array material. In addition, as the nanopatterned lenses were coated with HA during the fabrication process, their transmittance was calculated through simulation (Figure S9e,f). The deposition of HA coating reduced the transmission of visible light, most markedly for the TM mode. Figure 4b shows the results obtained for TM and TE modes passing through various Al thicknesses ($t$). In the TM mode, transmission in the visible region (400 nm < $\lambda$ < 780 nm) exceeded the average of 60% for 80 nm < $t$ < 100 nm. In the TE mode, the transmission was below 20% for $t$ > 60 nm, indicating excellent blocking performance. Therefore, an Al nanoline array, with $L/S$ = 100 nm/100 nm and $t$ = 90 nm, was adopted as the polarizer model for this application.

Two different images were used to confirm selective transmission according to the polarization mode (Figure 4c). These two images overlapped on the screen (Figure 4d); however, only one image was selectively transmitted through the nanopatterned contact lens (Figure 4e,f). Depending on the direction of nanopatterns on the lens, the overlapped image on the screen was selectively transmitted through the lens because of the polarization effect, due to which a stereoscopic effect based on binocular parallax could be realized using images taken from the left and right directions of the same object. The detailed setup used to confirm the stereoscopic effect due to binocular parallax is discussed in Experimental Section and shown in Figure S10. The images obtained from the left and right views (Figure 4g) were projected as polarized images in the TM and TE modes through two projectors. Depending on the direction of the contact lens nanopattern, only the TM mode image was transmitted, while the TE mode image was blocked to obtain a selectively transmitted image (Figure 4h). To evaluate the stereoscopic performance, the


https://doi.org/10.1021/acsami.1c06225
ACS Appl. Mater. Interfaces 2021, 13, 35069–35078

images obtained through the fabricated stereoscopic lenses were used to acquire distance information on the image by introducing a depth map (Figure 4i). The depth map is an image containing the distance information on objects; it is acquired based on the principle that images of farther objects, captured from two different horizontal viewpoints, have a smaller difference (calculated by comparing the pixels to evaluate similarity) between them.[47] The resulting depth map showed that the bell was the closest object, while the cable reel was the farthest one. Thus, the image was successfully separated through the lens, which allowed a 3D visualization effect using binocular parallax. In contrast to existing stereoscopic glasses, which suffer from image distortion at their edges, the proposed stereoscopic lens covers the entire eye, thereby eliminating viewing angle limitations and providing a deep sense of immersion.

**Cutoff Filter with a Nanodot Array.** In another application, we fabricated a functional lens that blocks/transmits a specific wavelength range using Ag nanodot array with a sharp transmission peak. Figure 5a–c shows the transmission spectra and SEM images of two different Ag nanodot patterns. Notably, as the transmission of the metallic nanostructure is due to its surface plasmon resonance,[28] the related transmission peak is a function of the nanostructure geometry (e.g., shape, size, and periodicity). The model used in this application was designed to have a peak curve that rapidly decreases with transmission at a specific wavelength, as presented in the FDTD simulation results shown in Figure S11a. The observed slight difference between the experimental and simulation results could be attributed to the variations in the material optical properties and imperfections of the fabricated samples, i.e., the samples did not have the ideal geometries for the numerical simulation. However, the simulation results provide guidelines for the geometric design of nanostructures with the desired optical characteristics, revealing that the blocked wavelength region depends on the diameter and pitch of the nanodot array and is usually red-shifted as the dot diameter and pitch increase and dot thickness decreases (Figure S11b–d). The model with $D/P$ = 200 nm/500 nm featured a high transmission of ≥80% at $\lambda$ < 650 nm. A possible application of our fabricated lens is the treatment of Irlen syndrome, which is a type of dyslexia caused by hypersensitivity to a certain wavelength of light.[48] It can be mitigated by blocking the light in the problem-causing wavelength range. Here this application was demonstrated using a red light-emitting diode (LED) with $\lambda$ = 600–650 nm. The Ag nanodot pattern with D/P = 180 nm/380 nm and $t$ = 50 nm had a less than 40% transmission at 600 nm < $\lambda$ < 670 nm (i.e., in the red-light region), blocking the light emitted by the red LED. Figure 5d–g shows the light transmitted through a conventional contact lens, whereas Figure 5h–k presents the results obtained for the nanopatterned contact lens, revealing that the latter lens effectively blocked red light but did not affect the transmission of light of other colors, such as green and blue. In the case of a white LED, there is minimal difference between the two lenses, as red light accounts for a small fraction of the overall emission spectrum. These results confirmed the ability of the patterned lens to block light within a specific wavelength range. By changing the pattern geometry (i.e., thickness, diameter, and pitch), wavelength ranges, such as those that correspond to ultraviolet (UV) or blue light and are potentially harmful to the eyes, could be selectively blocked.

## CONCLUSIONS

Herein we proposed a new method for the biocompatible nanotransfer printing of various functional nanopatterns onto HA films by exploiting the ability of HA to attract ambient moisture and form water bridges between polymer chains. According to the developed methodology, FM was placed on the hydrated, deformable, and sticky HA film and transferred to the film by applying external heat energy to break the water bridges. The rupture of the water bridges resulted in the shrinkage of the HA film, leading to the formation of a firm bonding between the HA film and the FM due to mechanical interlocking. This technique can be applied to various materials (e.g., Al, Ag, Au, Ni, Cr, Cu, and $TiO_2$) with nanoscale to mesoscale patterns. To demonstrate its practical applicability, the nanopatterned HA film was transferred to a soft contact lens using its inherent moisture, and it was subsequently used to realize stereoscopy and as a cutoff filter for treating Irlen syndrome. Binocular parallax-induced stereoscopy was implemented using polarization caused by the even transmission/blocking of visible light through/by a periodic Al nanoline array. To verify this effect, a depth map was introduced. The distance information obtained through the nanopatterned lens from two images taken from different horizontal viewpoints was added. In addition, a specific wavelength range could be blocked depending on the nanopattern shape, as confirmed for two types of nanodot arrays. This application can be used to correct dyslexia in patients with Irlen syndrome, which is caused by hypersensitive reactions to certain colors. The proposed method can potentially be used to produce augmented reality contact lenses by transferring chiral metastructures with circular polarization characteristics to contact lenses. Furthermore, it is expected to allow the biocompatible and facile fabrication of various functional devices on organs, bioimplantable devices, biosignal monitoring sensors, and drug delivery devices. For biomedical applications, functional structures should be long-lasting in wet or ionic environments, which was not investigated in this study. To obtain the short term and long-term stabilities, systematic studies on the passivation layers, which are biocompatible, chemically resistant, and do not alter the optical and electrical functionalities of the patterned functional materials, should be carried out in the future.

## EXPERIMENTAL SECTION

**Fabrication of Si Master with Nanoscale Patterns.** The Si master with nanoscale patterns was fabricated by KrF optical lithography and reactive ion etching. It was subsequently treated with trichloro(1*H*,1*H*,2*H*,2*H*-perfluorooctyl)silane (Sigma-Aldrich, St. Louis, MO) to separate the resin during the pattern replication process.

**Replication of the Si Master on the Polymer Film.** The polymer mold fabrication was carried out according to a previously reported procedure (Figure S12).[12] To replicate the patterns, a UV-curable PUA resin (311-RM, Munuta Technology Co., Ltd., Korea) was drop-cast onto a Si wafer. The Si master with resin was covered with a polyethylene terephthalate film as the supporting layer. Pressure was applied using a roller to remove the trapped air and fill the pattern with the resin. Finally, the Si master containing the resin was cured with UV light (2 × 90 s).

**FM Deposition on the PUA Mold.** FMs were deposited on the PUA mold using e-beam evaporation (Daeki Hi-Tech Co. Ltd., Korea) at a rate of 1.5–2 Å $s^{-1}$ under high vacuum (~$10^{-6}$ Torr).

**Fabrication of HA Film.** A suspension of HA powder (HA-TLM 20–40 (200–400 kDa); Bloomage Biotechnology Corporation Ltd.,


https://doi.org/10.1021/acsami.1c06225
ACS Appl. Mater. Interfaces 2021, 13, 35069–35078

China) in deionized water was stirred at 550 rpm for 4 h at room temperature (23 °C) to prepare a 1 wt % solution, which was then poured into a Petri dish fixed with a 2″ bare Si wafer. The dish was placed in a vacuum chamber for 10 min to remove air bubbles and dried at 50 °C in a convection oven for 1 day. After the removal of the Si wafer, the sample was fixed on a 4″ Si wafer and treated with $O_2$ plasma for 30 s. For sufficient hydration, the HA film was placed in a closed container next to a 2″ Petri dish filled with hot water, which ensured that at least 60% humidity was maintained inside the container.

**Nanotransfer Printing on HA Film.** The PUA mold, containing the deposited FM, and the hydrated HA film were stacked and attached together. The mold was subsequently pressurized for 5 min at ∼3 bar and 100 °C, cooled, and then separated from the HA film.

**Peel Test of the Transferred HA Film.** Because the fabricated HA film was very thin (∼20 μm), it was fixed on the PET film using Loctite 401 adhesive. For the peel test, tapes of various strengths, such as 3M Magic Tape to 3M VHB, were used.

**Nanotransfer Printing on Contact Lens.** A soft contact lens (1-DAY ACUVUE TruEye, Johnson & Johnson Vision Care, Inc., Jacksonville, FL) was placed on a hard optical lens, with a curvature similar to that of the eye's cornea, as a support. The nanopatterned HA film with a diameter of 10 mm was placed in a direction in which the pattern was in contact with the lens to prevent the sudden expansion of HA upon exposure to the contact lens moisture.

**Transmission Measurement.** The optical properties were investigated by a spectrometer (QE Pro 6000, Ocean Optics, Dunedin, FL). The glass wafer and contact lens attached to the optical lens were designated as references for the optical characterization of the nanopatterned HA film and nanopatterned contact lens, respectively.

**Numerical Simulation of Nanopattern Transmission.** FDTD simulation method (FDTD Solutions, Lumerical Inc., Canada) was used to compute the transmission of light through the polarizer model and nanodot array. To avoid interference due to reflection, perfectly matched layers were placed on the top and bottom, and a periodic boundary condition was defined by dividing the mesh at 3 nm intervals. The simulated values were determined by placing the source, designed structure, and monitor in sequence. The polarization and nanodot array models are shown in Figures S9 and S11, respectively.

**Experimental Setup for Stereoscopy.** The experimental setup used for stereoscopy is presented in Figure S8. Commercial films with different polarization directions were placed in front of two beam projectors so that only polarized light from the projector could be transmitted. The polarized light from the two projectors was directed at a reflective screen and transmitted to the fabricated lens. The transmitted images were acquired by a camera by changing the lens orientation by 90°.

**Specific Wavelength Blocking Experiment.** A voltage of 1.85 V was applied to a high-brightness red LED with a diameter of 5 mm. First, a nanopatterned HA film and then a contact lens were placed between the LED and wall. The transmitted light was captured with a camera.

**Surface and Cross-sectional Imaging.** Field emission SEM (Sirion, Thermo Fisher Scientific, Inc., Waltham, MA) and FIB microscopy (Helios Nanolab, Thermo Fisher Scientific, Inc., Waltham, MA) were performed to obtain high-resolution surface and cross-sectional images, respectively.

## ■ ASSOCIATED CONTENT

### Supporting Information

The Supporting Information is available free of charge at https://pubs.acs.org/doi/10.1021/acsami.1c06225.

Figures S1−S12 as described in the text (PDF)

## ■ AUTHOR INFORMATION


### Corresponding Authors

**Jun-Ho Jeong** − *Department of Nano Manufacturing Technology, Korea Institute of Machinery and Materials (KIMM), Daejeon 34103, South Korea;* orcid.org/0000-0003-0671-0225; Email: jhjeong@kimm.ac.kr

**Inkyu Park** − *Department of Mechanical Engineering, Korea Advanced Institute of Science and Technology (KAIST), Daejeon 34141, South Korea;* orcid.org/0000-0001-5761-7739; Email: inkyu@kaist.ac.kr

### Authors

**Jiwoo Ko** − *Department of Mechanical Engineering, Korea Advanced Institute of Science and Technology (KAIST), Daejeon 34141, South Korea; Department of Nano Manufacturing Technology, Korea Institute of Machinery and Materials (KIMM), Daejeon 34103, South Korea*

**Hyeok Joong Kang** − *Department of Nano Manufacturing Technology, Korea Institute of Machinery and Materials (KIMM), Daejeon 34103, South Korea*

**Junseong Ahn** − *Department of Mechanical Engineering, Korea Advanced Institute of Science and Technology (KAIST), Daejeon 34141, South Korea; Department of Nano Manufacturing Technology, Korea Institute of Machinery and Materials (KIMM), Daejeon 34103, South Korea;* orcid.org/0000-0002-4090-5440

**Zhi-Jun Zhao** − *Department of Nano Manufacturing Technology, Korea Institute of Machinery and Materials (KIMM), Daejeon 34103, South Korea*

**Yongrok Jeong** − *Department of Nano Manufacturing Technology, Korea Institute of Machinery and Materials (KIMM), Daejeon 34103, South Korea*

**Soon Hyoung Hwang** − *Department of Nano Manufacturing Technology, Korea Institute of Machinery and Materials (KIMM), Daejeon 34103, South Korea*

**Moonjeong Bok** − *Department of Nano Manufacturing Technology, Korea Institute of Machinery and Materials (KIMM), Daejeon 34103, South Korea*

**Sohee Jeon** − *Department of Nano Manufacturing Technology, Korea Institute of Machinery and Materials (KIMM), Daejeon 34103, South Korea*

**Jimin Gu** − *Department of Mechanical Engineering, Korea Advanced Institute of Science and Technology (KAIST), Daejeon 34141, South Korea*

**Ji-Hwan Ha** − *Department of Mechanical Engineering, Korea Advanced Institute of Science and Technology (KAIST), Daejeon 34141, South Korea; Department of Nano Manufacturing Technology, Korea Institute of Machinery and Materials (KIMM), Daejeon 34103, South Korea*

**Junsuk Rho** − *Department of Chemical Engineering and Department of Mechanical Engineering, Pohang University of Science and Technology (POSTECH), Pohang-si, Gyeongsangbuk-do 37673, South Korea;* orcid.org/0000-0002-2179-2890

Complete contact information is available at: https://pubs.acs.org/10.1021/acsami.1c06225


### Author Contributions

The manuscript was written through contributions from all authors. J.K. performed the experiments, analyzed the data, and wrote the paper. J.K., H.-J.K., S.H.H, S.J., and J.R. discussed the results of optical experiments and FDTD simulation. J.A., Z.-J.Z., Y.J., M.B., and J.G. discussed the mechanism and results of



https://doi.org/10.1021/acsami.1c06225
ACS Appl. Mater. Interfaces 2021, 13, 35069−35078

nanotransfer printing onto the contact lens. J.-H.J. and I.P. contributed to the overall direction of the project. All authors have approved the final version of the manuscript.

### Notes

The authors declare no competing financial interest.

## ■ ACKNOWLEDGMENTS

This work was supported by the National Research Foundation of Korea (NRF) grant funded by the Korean government, Ministry of Science, ICT and Future Planning (MSIP; no. 2015R1A5A1037668) and Center for Advanced Meta-Materials (CAMM) funded by the Ministry of Science, ICT and Future Planning, Korea, through the Global Frontier Project (CAMM; no. 2014M3A6B3063707).

## ■ ABBREVIATIONS

HA, hyaluronic acid; FMs, functional materials; PUA, polyurethane acrylate; SEM, scanning electron microscopy; *D*/*P*, diameter/pitch; *L*/*S*, line width/spacing; TE, transverse electric; TM, transverse magnetic; FIB, focused ion beam; 3D, three-dimensional; FDTD, finite-difference time-domain; LED, light-emitting diode; UV, ultraviolet

## ■ REFERENCES

(1) Park, J.; Jeong, Y.; Kim, J.; Gu, J.; Wang, J.; Park, I. Biopsy Needle Integrated with Multi-Modal Physical/Chemical Sensor Array. *Biosens. Bioelectron.* **2020**, *148*, 111822.

(2) Park, J.; Sempionatto, J. R.; Kim, J.; Jeong, Y.; Gu, J.; Wang, J.; Park, I. Microscale Biosensor Array Based on Flexible Polymeric Platform toward Lab-on-a-Needle: Real-Time Multiparameter Biomedical Assays on Curved Needle Surfaces. *ACS Sensors* **2020**, *5* (5), 1363−1373.

(3) Jeong, Y.; Park, J.; Lee, J.; Kim, K.; Park, I. Ultrathin, Biocompatible, and Flexible Pressure Sensor with a Wide Pressure Range and Its Biomedical Application. *ACS Sensors* **2020**, *5* (2), 481−489.

(4) Lee, H.; Song, C.; Hong, Y. S.; Kim, M. S.; Cho, H. R.; Kang, T.; Shin, K.; Choi, S. H.; Hyeon, T.; Kim, D. H. Wearable/Disposable Sweat-Based Glucose Monitoring Device with Multistage Transdermal Drug Delivery Module. *Sci. Adv.* **2017**, *3* (3), e1601314.

(5) Lee, H.; Song, C.; Baik, S.; Kim, D.; Hyeon, T.; Kim, D. H. Device-Assisted Transdermal Drug Delivery. *Adv. Drug Delivery Rev.* **2018**, *127*, 35−45.

(6) Koo, J.; Kim, S. B.; Choi, Y. S.; Xie, Z.; Bandodkar, A. J.; Khalifeh, J.; Yan, Y.; Kim, H.; Pezhouh, M. K.; Doty, K.; Lee, G.; Chen, Y. Y.; Lee, S. M.; D'Andrea, D.; Jung, K.; Lee, K. H.; Li, K.; Jo, S.; Wang, H.; Kim, J. H.; Kim, J.; Choi, S. G.; Jang, W. J.; Oh, Y. S.; Park, I.; Kwak, S. S.; Park, J. H.; Hong, D.; Feng, X.; Lee, C. H.; Banks, A.; Leal, C.; Lee, H. M.; Huang, Y.; Franz, C. K.; Ray, W. Z.; MacEwan, M.; Kang, S. K.; Rogers, J. A. Wirelessly Controlled, Bioresorbable Drug Delivery Device with Active Valves That Exploit Electrochemically Triggered Crevice Corrosion. *Sci. Adv.* **2020**, *6* (35), eabb1093.

(7) Han, M.; Wang, H.; Yang, Y.; Liang, C.; Bai, W.; Yan, Z.; Li, H.; Xue, Y.; Wang, X.; Akar, B.; Zhao, H.; Luan, H.; Lim, J.; Kandela, I.; Ameer, G. A.; Zhang, Y.; Huang, Y.; Rogers, J. A. Three-Dimensional Piezoelectric Polymer Microsystems for Vibrational Energy Harvesting, Robotic Interfaces and Biomedical Implants. *Nat. Electron.* **2019**, *2* (1), 26−35.

(8) Kim, D. H.; Lu, N.; Ghaffari, R.; Kim, Y. S.; Lee, S. P.; Xu, L.; Wu, J.; Kim, R. H.; Song, J.; Liu, Z.; Viventi, J.; De Graff, B.; Elolampi, B.; Mansour, M.; Slepian, M. J.; Hwang, S.; Moss, J. D.; Won, S. M.; Huang, Y.; Litt, B.; Rogers, J. A. Materials for Multifunctional Balloon Catheters with Capabilities in Cardiac Electrophysiological Mapping and Ablation Therapy. *Nat. Mater.* **2011**, *10* (4), 316−323.

(9) Humar, M.; Kwok, S. J. J.; Choi, M.; Yetisen, A. K.; Cho, S.; Yun, S. H. Toward Biomaterial-Based Implantable Photonic Devices. *Nanophotonics* **2017**, *6* (2), 414−434.

(10) Sreenivasan, S. V. Nanoimprint Lithography Steppers for Volume Fabrication of Leading-Edge Semiconductor Integrated Circuits. *Microsystems Nanoeng.* **2017**, *3* (1), 1−19.

(11) Ansari, M. A.; Kim, I.; Rukhlenko, I. D.; Zubair, M.; Yerci, S.; Tauqeer, T.; Mehmood, M. Q.; Rho, J. Engineering Spin and Antiferromagnetic Resonances to Realize an Efficient Direction-Multiplexed Visible Meta-Hologram. *Nanoscale Horizons* **2020**, *5* (1), 57−64.

(12) Ko, J.; Zhao, Z. J.; Hwang, S. H.; Kang, H. J.; Ahn, J.; Jeon, S.; Bok, M.; Jeong, Y.; Kang, K.; Cho, I.; Jeong, J. H.; Park, I. Nanotransfer Printing on Textile Substrate with Water-Soluble Polymer Nanotemplate. *ACS Nano* **2020**, *14* (2), 2191−2201.

(13) Bowman, S.; Awad, M. E.; Hamrick, M. W.; Hunter, M.; Fulzele, S. Recent Advances in Hyaluronic Acid Based Therapy for Osteoarthritis. *Clin. Transl. Med.* **2018**, *7* (1), 6.

(14) Rohrich, R. J.; Bartlett, E. L.; Dayan, E. Practical Approach and Safety of Hyaluronic Acid Fillers. *Plastic and Reconstructive Survery Global Open* **2019**, *7* (6), e2172.

(15) Knopf-Marques, H.; Pravda, M.; Wolfova, L.; Velebny, V.; Schaaf, P.; Vrana, N. E.; Lavalle, P. Hyaluronic Acid and Its Derivatives in Coating and Delivery Systems: Applications in Tissue Engineering, Regenerative Medicine and Immunomodulation. *Adv. Healthcare Mater.* **2016**, *5* (22), 2841−2855.

(16) Zhu, J.; Tang, X.; Jia, Y.; Ho, C. T.; Huang, Q. Applications and Delivery Mechanisms of Hyaluronic Acid Used for Topical/Transdermal Delivery − A Review. *Int. J. Pharm.* **2020**, *578*, 119127.

(17) Fallacara, A.; Baldini, E.; Manfredini, S.; Vertuani, S. Hyaluronic Acid in the Third Millennium. *Polymers (Basel, Switz.)* **2018**, *10* (7), 701.

(18) Suh, K. Y.; Khademhosseini, A.; Yang, J. M.; Eng, G.; Langer, R. Soft Lithographic Patterning of Hyaluronic Acid on Hydrophilic Substrates Using Molding and Printing. *Adv. Mater.* **2004**, *16* (7), 584−588.

(19) Li, M.; Mondrinos, M. J.; Chen, X.; Gandhi, M. R.; Ko, F. K.; Lelkes, P. I. Elastin Blends for Tissue Engineering Scaffolds. *J. Biomed. Mater. Res., Part A* **2006**, *79* (4), 963−973.

(20) Jouon, N.; Rinaudo, M.; Milas, M.; Desbrières, J. Hydration of Hyaluronic Acid as a Function of the Counterion Type and Relative Humidity. *Carbohydr. Polym.* **1995**, *26* (1), 69−73.

(21) Burke, S. E.; Barrett, C. J. Swelling Behavior of Hyaluronic Acid/Polyallylamine Hydrochloride Multilayer Films. *Biomacromolecules* **2005**, *6* (3), 1419−1428.

(22) Yao, S.; Wang, X.; Liu, X.; Wang, R.; Deng, C.; Cui, F. Effects of Ambient Relative Humidity and Solvent Properties on the Electrospinning of Pure Hyaluronic Acid Nanofibers. *J. Nanosci. Nanotechnol.* **2013**, *13* (7), 4752−4758.

(23) Zhao, Z. J.; Hwang, S. H.; Jeon, S.; Jung, J. Y.; Lee, J.; Choi, D. G.; Choi, J. H.; Park, S. H.; Jeong, J. H. Effects of Polymer Surface Energy on Morphology and Properties of Silver Nanowire Fabricated via Nanoimprint and E-Beam Evaporation. *Appl. Surf. Sci.* **2017**, *420*, 429−438.

(24) Zhao, Z. J.; Shin, S. H.; Choi, D. G.; Park, S. H.; Jeong, J. H. Shape-Controlled 3D Periodic Metal Nanostructures Fabricated via Nanowelding. *Small* **2018**, *14* (6), 1703102.

(25) Park, J.; Kim, J.; Kim, S. Y.; Cheong, W. H.; Jang, J.; Park, Y. G.; Na, K.; Kim, Y. T.; Heo, J. H.; Lee, C. Y.; Lee, J. H.; Bien, F.; Park, J. U. Soft, Smart Contact Lenses with Integrations of Wireless Circuits, Glucose Sensors, and Displays. *Sci. Adv.* **2018**, *4* (1), eaap9841.

(26) Chiou, J. C.; Hsu, S. H.; Huang, Y. C.; Yeh, G. T.; Liou, W. T.; Kuei, C. K. A Wirelessly Powered Smart Contact Lens with Reconfigurable Wide Range and Tunable Sensitivity Sensor Readout Circuitry. *Sensors* **2017**, *17* (1), 108.

(27) Leonardi, M.; Pitchon, E. M.; Bertsch, A.; Renaud, P.; Mermoud, A. Wireless Contact Lens Sensor for Intraocular Pressure



https://doi.org/10.1021/acsami.1c06225
ACS Appl. Mater. Interfaces 2021, 13, 35069−35078

Monitoring: Assessment on Enucleated Pig Eyes. *Acta Ophthalmol.* **2009**, *87* (4), 433−437.
(28) Hwang, S. H.; Jeon, S.; Kim, M. J.; Choi, D. G.; Choi, J. H.; Jung, J. Y.; Kim, K. S.; Lee, J.; Jeong, J. H.; Youn, J. R. Covalent Bonding-Assisted Nanotransfer Lithography for the Fabrication of Plasmonic Nano-Optical Elements. *Nanoscale* **2017**, *9* (38), 14335−14346.
(29) Lee, J. O.; Park, H.; Du, J.; Balakrishna, A.; Chen, O.; Sretavan, D.; Choo, H. A Microscale Optical Implant for Continuous in Vivo Monitoring of Intraocular Pressure. *Microsystems Nanoeng.* **2017**, *3* (April), 1−9.
(30) Lee, M. S.; Lee, K.; Kim, S. Y.; Lee, H.; Park, J.; Choi, K. H.; Kim, H. K.; Kim, D. G.; Lee, D. Y.; Nam, S.; Park, J. U. High-Performance, Transparent, and Stretchable Electrodes Using Graphene-Metal Nanowire Hybrid Structures. *Nano Lett.* **2013**, *13* (6), 2814−2821.
(31) Liao, Y.-T.; Yao, H.; Lingley, A.; Parviz, B.; Otis, B. P. A 3-$\mu$W CMOS Glucose Sensor for Wireless Contact-Lens Tear Glucose Monitoring. *IEEE J. Solid-State Circuits* **2012**, *47* (1), 335−344.
(32) Tang, H.; Alqattan, B.; Jackson, T.; Pikramenou, Z.; Sun, X. W.; Wang, K.; Butt, H. Cost-Efficient Printing of Graphene Nanostructures on Smart Contact Lenses. *ACS Appl. Mater. Interfaces* **2020**, *12* (9), 10820−10828.
(33) Alqattan, B.; Yetisen, A. K.; Butt, H. Direct Laser Writing of Nanophotonic Structures on Contact Lenses. *ACS Nano* **2018**, *12* (6), 5130−5140.
(34) Paik, S.; Kim, G.; Chang, S.; Lee, S.; Jin, D.; Jeong, K. Y.; Lee, I. S.; Lee, J.; Moon, H.; Lee, J.; Chang, K.; Choi, S. S.; Moon, J.; Jung, S.; Kang, S.; Lee, W.; Choi, H. J.; Choi, H.; Kim, H. J.; Lee, J. H.; Cheon, J.; Kim, M.; Myoung, J.; Park, H. G.; Shim, W. Near-Field Sub-Diffraction Photolithography with an Elastomeric Photomask. *Nat. Commun.* **2020**, *11* (1), 805.
(35) Jeong, J. W.; Arnob, M. M. P.; Baek, K. M.; Lee, S. Y.; Shih, W. C.; Jung, Y. S. 3D Cross-Point Plasmonic Nanoarchitectures Containing Dense and Regular Hot Spots for Surface-Enhanced Raman Spectroscopy Analysis. *Adv. Mater.* **2016**, *28* (39), 8695−8704.
(36) Elsherif, M.; Hassan, M. U.; Yetisen, A. K.; Butt, H. Wearable Contact Lens Biosensors for Continuous Glucose Monitoring Using Smartphones. *ACS Nano* **2018**, *12* (6), 5452−5462.
(37) Kim, J.; Kim, M.; Lee, M. S.; Kim, K.; Ji, S.; Kim, Y. T.; Park, J.; Na, K.; Bae, K. H.; Kim, H. K.; Bien, F.; Lee, C. Y.; Park, J. U. Wearable Smart Sensor Systems Integrated on Soft Contact Lenses for Wireless Ocular Diagnostics. *Nat. Commun.* **2017**, *8*, 14997.
(38) Nazarov, A.; Knyazer, B.; Lifshitz, T.; Schvartzman, M.; Abdulhalim, I. Assessment of Intraocular Pressure Sensing Using an Implanted Reflective Flexible Membrane. *J. Biomed. Opt.* **2017**, *22* (4), 047001.
(39) Zhang, Y.; Chen, Y.; Man, T.; Huang, D.; Li, X.; Zhu, H.; Li, Z. High Resolution Non-Invasive Intraocular Pressure Monitoring by Use of Graphene Woven Fabrics on Contact Lens. *Microsystems Nanoeng.* **2019**, *5* (1), 39.
(40) Mansouri, K.; Medeiros, F. A.; Tafreshi, A.; Weinreb, R. N. Continuous 24-h Monitoring of Intraocular Pressure Patterns with Contact Lens Sensor: Safety, Tolerability, and Reproducibility in Patients with Glaucoma. *Arch. Ophthalmol.* **2012**, *130* (12), 1534−1539.
(41) Maulvi, F. A.; Shaikh, A. A.; Lakdawala, D. H.; Desai, A. R.; Pandya, M. M.; Singhania, S. S.; Vaidya, R. J.; Ranch, K. M.; Vyas, B. A.; Shah, D. O. Design and Optimization of a Novel Implantation Technology in Contact Lenses for the Treatment of Dry Eye Syndrome: In Vitro and in Vivo Evaluation. *Acta Biomater.* **2017**, *53*, 211−221.
(42) Lee, S.; Jo, I.; Kang, S.; Jang, B.; Moon, J.; Park, J. B.; Lee, S.; Rho, S.; Kim, Y.; Hong, B. H. Smart Contact Lenses with Graphene Coating for Electromagnetic Interference Shielding and Dehydration Protection. *ACS Nano* **2017**, *11* (6), 5318−5324.
(43) Badawy, A. R.; Hassan, M. U.; Elsherif, M.; Ahmed, Z.; Yetisen, A. K.; Butt, H. Contact Lenses for Color Blindness. *Adv. Healthcare Mater.* **2018**, *7* (12), 1800152.
(44) Karepov, S.; Ellenbogen, T. Metasurface-Based Contact Lenses for Color Vision Deficiency. *Opt. Lett.* **2020**, *45* (6), 1379−1382.
(45) Ketelson, H. A.; Meadows, D. L.; Stone, R. P. Dynamic Wettability Properties of a Soft Contact Lens Hydrogel. *Colloids Surf., B* **2005**, *40* (1), 1−9.
(46) Moreddu, R.; Vigolo, D.; Yetisen, A. K. Contact Lens Technology: From Fundamentals to Applications. *Adv. Healthcare Mater.* **2019**, *8* (15), 1900368.
(47) Abbeloos, W. Stereo Matching, MATLAB Central File Exchange. https://www.mathworks.com/matlabcentral/fileexchange/28522-stereo-matching (accessed Oct 5, 2020).
(48) Kriss, I.; Evans, B. J. W. The Relationship between Dyslexia and Meares-Irlen Syndrome. *Journal of Research in Reading* **2005**, *28* (3), 350−364.


https://doi.org/10.1021/acsami.1c06225
*ACS Appl. Mater. Interfaces* 2021, 13, 35069−35078